Express Polymer Letters Vol.17, No.8 (2023) 806–818
Available online at www.expresspolymlett.com
https://doi.org/10.3144/expresspolymlett.2023.60

Research article

Electromechanical characterizations of PEDOT:PSS and its nanocomposite thin films on a cost-effective polymer substrate for microelectromechanical systems (MEMS) applications

Shehroze Tahir Khan, Murtuza Mehdi[*], Tariq Jamil

Department of Mechanical Engineering NED University of Engineering & Technology Karachi, University Road, 75270 Karachi, Pakistan.

Received 31 January 2023; accepted in revised form 22 April 2023

Abstract. Conductive polymer poly(3,4-ethylenedioxythiophene):poly(styrenesulfonate) PEDOT:PSS is the most widely used material in stretchable and flexible electronics not only due to its good electrical and mechanical properties but also its use in numerous biomedical sensing applications. This article investigates the electromechanical behavior of PEDOT:PSS and its nanocomposite thin film. The films were rod-coated on a chemically treated, cost-effective single-component polymer that was previously characterized as an alternative available substrate material for stretchable and flexible microelectromechanical systems (MEMS) based devices. The results show that the films exhibit stable resistive behavior in response to various applied mechanical loads such as stretching, twisting, combined stretching, and twisting and forced vibrations. The films also show good thermal stability at relatively high temperatures. The prepared films also reveal their applicability as thermal actuators. It was also found that adding nanophases of silver material in PEDOT:PSS enhances the performance of thin films. These results also suggest that the rod-coated PEDOT:PSS and its composite thin films may have versatile applications like stretchable, twistable, and vibration-tolerant conductors, thermal actuators, and devices for future low-cost MEMS devices.

Keywords: *polymer composites, adhesion, rod-coating, microelectromechanical, material testing*

1. Introduction

In the last few years, substrate-bonded, electrically functional thin films have emerged as the most popular application in stretchable and flexible electronic devices. This is because modern electronic applications demand high-performance devices that can perform exceptionally well at various types of mechanical loadings [1–4]. These applications include stretchable and flexible conductors, sensors, energy harvesting, and storage devices [5–12], *etc.* These devices are usually made by depositing functional films on soft rubber-like stretchable and flexible substrates [9, 13–15]. Among these combinations, conductive polymer poly(3,4-ethylenedioxythiophene)/poly(styrenesulfonate) (PEDOT:PSS) deposited on polydimethyl siloxane (PDMS) is the most popular one [14, 16–19]. Many researchers have reported the experimental findings of this polymer-polymer laminate fabricated through different techniques. However, the results reported in these studies are more inclined towards the material characterizations, while the mechanical aspects were less explored [17, 19–22]. Also, in most of these studies, researchers used PDMS as the substrate material, and the devices were only tested for stretching and bending loads at low strain rates [16, 17, 23]. Furthermore, the intensive

[*]Corresponding author, e-mail: drmurtuza@neduet.edu.pk

use of PDMS in these devices has increased its demand. Secondly, the prevailing conditions of the recent pandemic have compelled researchers to search for alternate, low-cost and easily fetchable materials for the realization of stretchable and flexible MEMS devices.

Therefore, in this work, we have reported experimental results related to pristine PEDOT:PSS and its nanocomposite thin films. These films were fabricated through a non-vacuum-based rod coating technique on a millimeter-thick, single-component silicone-based polymer substrate. This polymer is easily available, low-cost, and commonly used as a sealant. The characterizations of this material and its application in stretchable thin films are described in our recent work [24]. Like PDMS, this silicone-based polymer is also hydrophobic. Therefore, a proper surface treatment is required before depositing the thin film material. To overcome this problem, different types of surface treatment methods are reported. These include UV ozone cleaning [25], acid etching [26], random roughness generation [27], surface grating and patterning [28] and chemical treatment [29, 30]. Among these methods, chemical treatment gave better lasting results [30]. The prepared thin films are tested through complex mechanical tests on custom-built test equipment designed to test substrate-bonded thin films. These tests include stretching, twisting, combined stretching and twisting, cyclic stretching and bending, and vibration testing. In this work, mechanical tests were performed at relatively high deformation rates, thus making these tests more challenging and aggressive. The thermal response of the films and actuation of the laminates were also tested to observe the change in resistance and actuation response to temperature. The results showed that the prepared thin films performed exceptionally well on chemically treated polymer substrates. The results also suggested that adding a metal nano phase enhances the mechanical performance of PEDOT:PSS films which might be useful in future low-cost stretchable and flexible electronics applications like stretchable and flexible conductors, sensors, nanogenerators and actuators.

2. Experimental

2.1. Materials and equipments

Silicone-based room temperature vulcanized (RTV) polymer (BS-8599 V7, Bossil Technology, Selangor, Malaysia) was used as the substrate material. It is a

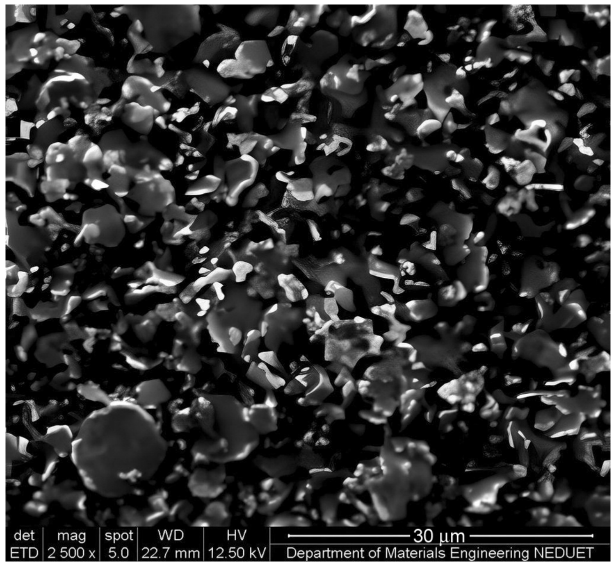

Figure 1. Scanning electron micrograph of silver ink containing silver nanoplatelets.

single-component polymer that comes in the form of paste. PEDOT:PSS was purchased as a thick paste from Sigma Aldrich (Belgium). *N*,*N*-dimethylformamide (*N*,*N*-DMF) was purchased from Merk Millipore (Darmstadt, Germany). Polyvinylpyrrolidone (PVP) (5295-100G) was purchased from Calbiochem, San Diego, CA, USA. Transparent nail polish was purchased from a local cosmetic supplier (BN Cosmetics, Pakistan). Silver conductive ink containing silver nanoplatelets was purchased from the local electronics market (Active Electronics, Pakistan). The presence of silver nanoplatelets was confirmed by scanning electron microscopy (SEM). Figure 1 shows the SEM image of silver ink containing silver nanoplatelets with average lateral dimensions of around 5.53 µm.

For viscosity measurements of prepared inks, an Ostwald viscometer was used. The electrical conductivity (EC) of the inks was measured by a pen-type digital EC meter (Originblue Technology, Ningbo, China) while for weight measurements, a precision electronic balance (Hefei Vetus Electronic Technology, Anhui, China) having the least count of 0.001 mg was used.

2.2. Preparation and treatment of RTV polymer substrate

RTV substrates of dimensions of 70×10×1.10 mm were prepared by casting RTV into an open mould. The mould was formed by pasting 1.10 mm thick glass slides on a 5 mm thick glass plate covered with cello tape. The polymer was applied to the mould cavity and levelled by dragging a cutter knife blade at an average velocity of 20 mm/s. This method ensures good thickness control along the length of the substrate with the least variation. The method was repeated for the entire mould. Afterwards, the samples were cured in an open atmosphere at 26 °C and 40% relative humidity for 1 to 2 hours. These protocols are necessary for curing since the single-component RTV polymers are supplied with pre-mixed curing agents [24]. Therefore, these silicones rely on atmospheric temperature and humidity for curing [31]. After curing, the samples were removed from the mould by applying a small amount of acetone at the polymer–mould interface. The acetone helps in the easy removal of the substrates without any damage.

To improve the surface adhesion, RTV substrates were chemically treated by immersing them in an aqueous solution of polyvinylpyrrolidone (PVP) (25 wt% concentration) for 18–24 hours. After the specified time, the samples were removed from the solution by wiping out the extra liquid using tissue paper. Finally, the samples were dried in ambient air for 15 to 20 minutes.

2.3. Preparation of PEDOT: PSS-based conductive inks

The pristine PEDOT:PSS ink was prepared by thoroughly mixing the PEDOT:PSS paste in *N*,*N*-DMF (50 wt% concentration). The solution was shaken for five minutes. Then clear nail polish was added to the ink at 48 wt% concentration. The DMF improves the electrical conductivity of the ink [4] while nail polish improves its applicability on smooth substrates [32–35]. The PEDOT:PSS nanocomposite ink was prepared by adding silver nanoplatelet ink in 5 wt% concentration to the pristine ink. The solution was shaken for five minutes to form a homogeneous solution. The physical properties of the as-synthesized inks were measured and are shown in Table 1.

2.4. Fabrication of pristine PEDOT:PSS and its nanocomposite films

The pristine PEDOT:PSS film was formed by dispensing 200 µl volume of synthesized ink on the substrate using a micropipette (Dlab Scientific, Beijing, China). The ink was spread by gently pulling a smooth stainless rod of diameter 2.5 mm at an average velocity of 10 mm/s. The samples were dried inside a convection oven at 95 °C for 10 minutes, after which the heating element turned off automatically while the circulation fan continued to run until the ambient temperature reached. After this intermediate step, another coat of ink (200 µl) was applied. The samples were dried again following the same protocols. The PEDOT:PSS nanocomposite films were prepared by following the same procedure. The samples were dried inside the convection oven at 100 °C for 15 min following the same protocols. After that, another coat of ink (200 µl) was applied, and the films were baked inside the oven. Finally, electrical contacts were made on the finished laminates using 0.18 mm pure enamel copper wire and silver conductive paste (Mechanic, MCN-DJ002, China). Figures 2a and 2b show the typical rod-coated PEDOT:PSS and PEDOT:PSS nanocomposite films while Figures 2c and 2d show the SEM cross-section of the substrate with the coated films. From different SEM images, the average thickness of the prepared films was found to be 50 µm.

Table 1. Physical properties of as-synthesized conductive inks used in this work.

Ink type	Density [kg/m^3]	Viscosity [mPa·s]	Electrical conductivity [µS/cm]
Pristine PEDOT:PSS ink	933	4.90	218
PEDOT:PSS nanocomposite ink	1016	4.85	705

2.5. Electromechanical characterizations

These types of characterizations are performed to measure changes in the macroscopic properties like resistance or capacitance of thin films as a function of applied mechanical strain [36–38]. For this purpose, two custom-built machines were used namely, a thin film tensile tester machine and a thin film vibration testing machine. The thin film tensile tester machine, shown in Figure 3, was capable of performing stretching, twisting, and bending tests using a moving clamp controlled by a precision lead screw and stepper drives (Oriental Motor, Japan). The vibration testing machine, shown in Figure 4, was used to vibrate the thin film sample through a 3D-printed cam driven by an encoder-based DC motor (Chihai Motor Co. Shenzhen, China). Both machines were controlled by an Arduino microcontroller and equipped with an auto-ranging ohm meter to record the resistance of the samples during the experiment. The accuracy of the meter was verified by a commercial digital multimeter (UNI-T 33D) and was found to be within ±1%. The testing data of the machines were recorded in real-time in Microsoft Excel through the Data Streamer plugin.

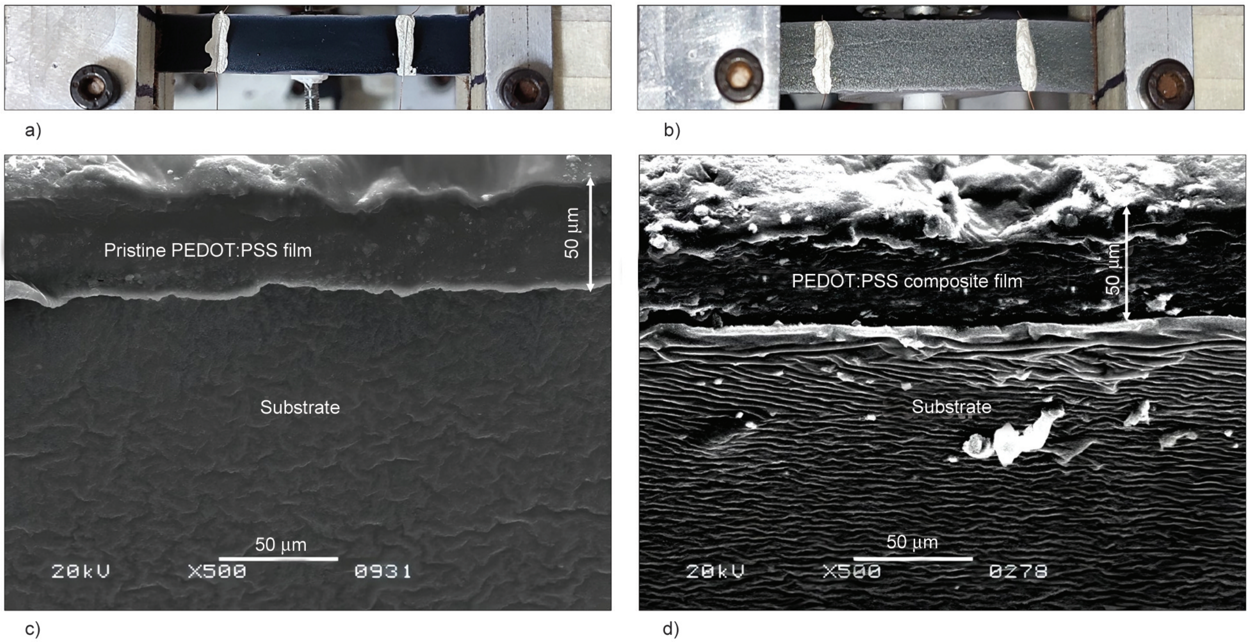

Figure 2. Rod coated PEDOT: PSS-based films on RTV substrate. a) pristine PEDOT:PSS laminate mounted on the testing rig with electrical contacts attached; b) PEDOT:PSS composite laminate mounted on characterization equipment for testing; c), d) lateral SEM images of PEDOT:PSS and its nanocomposite thin film laminates showing their cross-sectional dimensions.

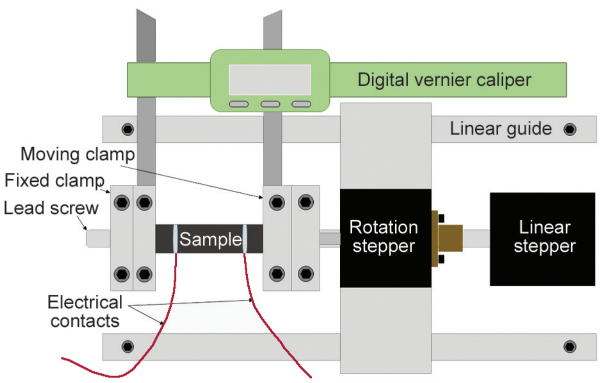

Figure 3. Schematic diagram of thin film tensile testing machine illustrating stretching test.

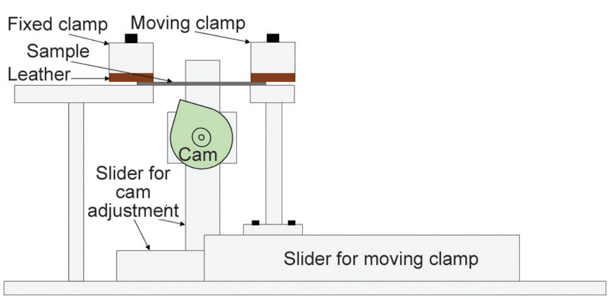

Figure 4. Schematic diagram of thin film vibration testing machine showing forced vibration testing of the sample, excited by a cam.

2.5.1. Stretching test

This test aims to test the stretchability of the thin films when subjected to uniaxial tensile load. The samples were mounted 10 mm from each side. A 3.5 mm thick piece of leather was used to provide a soft grip and minimize the residual stresses near the clamping surface. The samples were slowly straightened at a speed of 0.00625 mm/s and acceleration of 0.003125 mm/s^2. The gauge length was measured using a digital caliper (Insize, Co., Ltd., China) having the least count of 0.01 mm, and then electrical contacts were connected to the ohm meter. The samples were stretched at a speed of 0.0625 mm/s and acceleration of 0.03125 mm/s^2 up to the point of material failure. These input parameters yielded the strain rate of 2 s^{-1}, which is 1000 times higher than the previously reported works [16, 17, 23, 26, 39, 40]. The strain and resistance readings recorded by the machine were later converted into normalized resistance-strain data for analyzing the stretching behavior of pristine and composite thin films of PEDOT:PSS. The normalized resistance of the sample is calculated by dividing each value of resistance by the initial resistance of the sample at gauge length.

2.5.2. Twisting test

This test aims to determine the flexibility of thin film laminates when twisting loads are applied at large angles. During these tests, the linear stage was also locked to avoid errors. Two variations of the test were performed; one is called slow twisting, while the other is called fast twisting. In slow twisting, the samples were twisted at a speed of 0.5625°/s and acceleration of $0.28125°/s^2$. On the other hand, in fast twisting, the samples were twisted at 10.125°/s with an acceleration of $5.0625°/s^2$. The data captured by the machine was later converted into normalized resistance-twist angle curves to visualize the twisting behaviour of PEDOT:PSS and its nanocomposite thin film laminates.

2.5.3. Combined stretching and twisting test

This test is focused on testing the performance of pristine and composite thin films when uniaxial tensile and twisting loads are applied simultaneously. The test simulates the functionality of thin films as stretchable and twistable sensors, which may have potential applications in wearable electronic devices [41]. The samples were mechanically loaded up to material failure at a speed of 0.00625 mm/s and acceleration of $0.003125 mm/s^2$, with twisting parameters of 0.5625°/s and $0.28125°/s^2$ respectively. The results were later converted into normalized resistance curves to study the electromechanical behaviour of prepared films as a function of linear strain and twisting.

2.5.4. Cyclic stretching and bending test

These tests aim to check the reliability of the thin film laminates when cyclic tensile and bending loads are applied. In cyclic stretching, the samples undergo stretching and flexing cycles at 12% strain of their gauge lengths. On the other hand, in cyclic bending, the samples were bent to a minimum radius (~2 mm) and then flexed to their gauge length repeatedly. The speed and acceleration in cyclic stretching were 0.0625 mm/s and $0.03125 mm/s^2$ respectively. Whereas, in cyclic bending, these parameters were changed to 1.5625 mm/s and $1.09375 mm/s^2$. The tests were continued up to the point of material failure and the resistance and number of cycles were noted.

2.5.5. Vibration test

This test aims to test the functionality of substrate-bonded thin films when forced vibrations are applied. The sample was mounted according to the protocols described in Section 2.5.1. 3D printed cams of three different sizes, 0.5, 1, and 3 mm, were used to vibrate the sample from 0 to 45 Hz. The circular part of the cam was made to touch the sample base as a reference. After that, the cam motor slowly started and held at an rpm equivalent to 3 Hz for 90 s. Then the frequency of the cam increased by an increment of 3 Hz and held for another 90 s. The procedure continued until the film became electrically dysfunctional. The test was repeated on different cams with various samples to record the frequency–resistance data.

2.5.6. Thermal tests

The thermal tests were performed to check the resistive behavior and thermal actuation of the prepared laminates in response to the applied thermal gradient. Two types of tests were conducted. In the first test, samples of 35×10×1.1 mm size were used. The sample was fixed to a 1 mm thick glass slide via heat-resistant tape and placed on a hot plate. The electrical contacts of the sample were connected to the ohm meter for resistance measurements. A thermocouple was also attached to the assembly for temperature measurements. The temperature was slowly increased to 250 °C to observe the change in resistance of the laminate. Afterward, the hotplate was turned off, and the sample was allowed to cool at ambient. The temperatures and resistance were recorded during the heating and cooling cycles.

In the second test, a similar setup was used. This time, the sample was placed on a 6 mm thick glass plate with one end fixed only. A steel scale having a resolution of 0.05 mm was vertically fixed to the assembly for actuation measurements. The temperature was slowly increased, and the thermal actuation was noted. For each actuation measurement, the corresponding temperature was recorded to plot the temperature–height graph of the laminates.

3. Results and discussion

The mechanical performance of thin film laminates depends on various factors. These include stiffness, thickness and surface conditions of substrate [42–44], thickness of film [45, 46], film fabrication and sintering methods [47–50], deformation rates [16, 17, 23, 26, 39, 40], *etc.* The laminates used in this study are produced by depositing a functional film on a chemically treated smooth RTV substrate via rod coating. This substrate material is cost-effective and has similar mechanical properties compared to PDMS and was not explored previously in stretchable and flexible electronic applications. Also, new variations of electromechanical characterizations like slow and fast twisting and combined stretching and twisting are added, which were not previously explored by the researchers. Furthermore, the electromechanical characterizations performed in this study are more dynamic because of very high deformation rates; these factors contribute towards making this study unique. The following sections discuss the various findings of this work.

3.1. Electromechanical behaviour under stretching

Figure 5 shows the electromechanical response of the PEDOT:PSS and its nanocomposite films under stretching. It can be seen that the pristine films remain conductive up to 15% while composite films remain up to 17% strain. After that, both films crack and start delaminating from the substrate. At this point, it should be noted that these results are yielded at a higher stretching rate of 2 s^{-1} on a chemically treated smooth substrate. The normalized resistance of pristine films is 2.15 times the initial value (unstretched length), while that of composite films is 3.15. Also, the pristine films show a gradual change in resistance to failure. On the hand, the resistive behaviour of composite films can be split into two regions. In the first region, the normalized resistance is limited to 1.25 times the initial value. Therefore, this can be considered as a region of constant resistance. The stretchability in this region is extended up to 10% strain. This is due to the presence of silver nanoplatelets, which compensates for the change in resistance during stretching. This particular behaviour of the composite films is also important, as stretching, with minimal change in resistance, is one of the most important characteristics of stretchable electronics [18]. Furthermore, this region is also attributed to the capability of chemically treated RTV substrate which keeps the film bonded to the surface up to 10% strain. The second region starts after 10% strain. In this region, the resistance of the composite films starts increasing rapidly. In this region, the maximum normalized resistance is 3.93 times the initial resistance value; hence, the laminate behaves more like a stretchable resistor. This is due to the spreading of silver nanoplatelets in the laminate as the sample is stretched. This region continues up to 16% strain until a crack appears and propagates quickly. This results in the complete failure of the composite film.

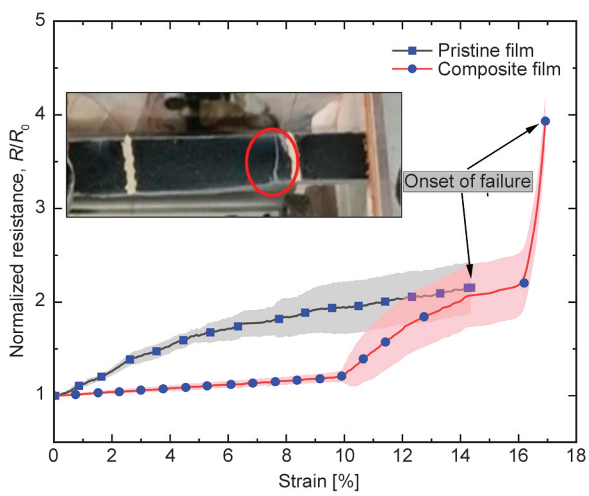

Figure 5. Variation of normalized resistance as a function of uniaxial stretching for rod-coated pristine PEDOT:PSS and its nanocomposite films on a chemically treated low-cost substrate. The inset shows the pristine PEDOT:PSS film stretched to complete failure. The arrows indicate the onset of material failure. Error bars with filled areas show the standard deviation for the set of experiments.

3.2. Electromechanical behaviour under twisting

Figure 6 shows the electromechanical response of the films when slow, and fast twisting is applied. It is clear that both films show very little change in resistance in slow twisting, 1.08 times the initial resistance for pristine films and 1.02 times for composite films at twisting angles of 349 and 360° for pristine and composite films, respectively. Whereas in fast twisting, the pristine films last up to 189° of twist angle while the composite films go up to 351° with minimal resistance change. This implies that the adhesion of the functional films on chemically treated substrates performs exceptionally well when controlled twisting loads are applied. Results from previous research suggested that exploitation of UV/ozone (UVO) treated or patterned rough substrates is more hydrophilic which means better electromechanical performance yet these methods add to the overall cost [18–20]. However, the laminates fabricated in this study utilize none of these techniques and the bonding between the functional films and smooth RTV substrate is exclusively due to surface wettability caused by chemical treatment with PVP. Overall, the composite films perform exceptionally well in twisting, which shows that the addition of silver nano phase improves the mechanical performance of PEDOT:PSS composite films. Therefore, these films can be used as bendable and twistable sensors in various MEMS-based applications and flexible electronic devices.

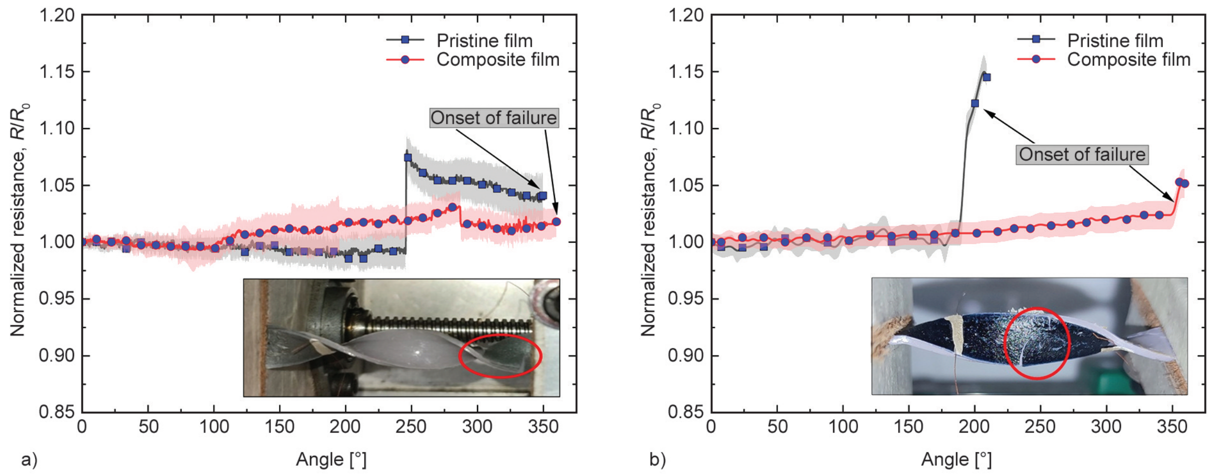

Figure 6. Variation of normalized resistance as a function of a) slow twisting, b) fast twisting for rod-coated pristine PEDOT:PSS and its nanocomposite films on a chemically treated low-cost substrate. The insets show the cracking and delamination of the composite and pristine films during slow and fast twisting, respectively. The arrows indicate the onset of material failure. Error bars with filled areas show the standard deviation for the set of experiments.

3.3. Electromechanical behavior under combined stretching and twisting

Figure 7 shows the combined stretching and twisting behavior of PEDOT:PSS and its nanocomposite films. On simultaneous stretching and twisting, the pristine films last only up to 1.94% strain at 84.4° twist angle, while the composite films last up to 4.86% at 218.3°. The maximum normalized resistance in pristine films goes up to 1.12 times the initial value, while that of composite films goes up to 1.04 times the initial normalized resistance. This behavior of pristine films can be split into two regions. In the first region, the normalized resistance remains close to one up to 0.47% strain around a 15° angle. It exhibits the capability of the pristine film laminates to work as stretchable and twistable sensors when operated within this small envelope. This region continued up to 1.6% strain and 65° twist angle. Afterward, the second region starts in which the laminates act more like a stretchable resistor. This change is caused by the deformation of pristine films, which continued up to 1.94% strain and 84.4° after which the film starts cracking and delaminating from the substrate. On the other hand, the composite films show linear response up to 4.4% strain and 197.6° angle. After which, the resistance increases abruptly due to cracking, and film delamination occurs. The delamination caused the unloading of the film from the substrate. Therefore, the normalized resistance becomes constant after this point. The reason for the reduced electromechanical performance of the laminates lies in the fact that the uniaxial stretching at dynamic

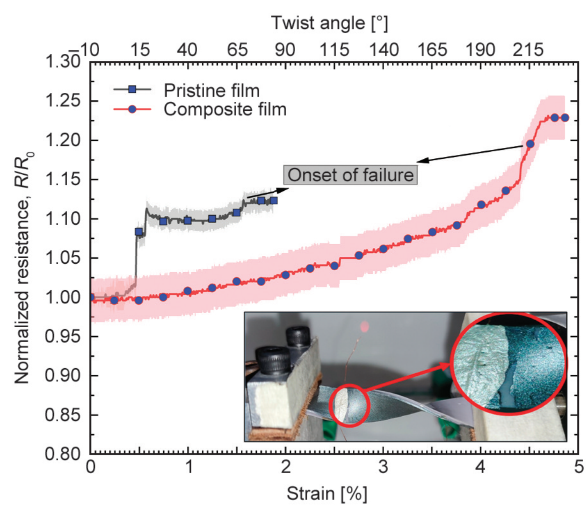

Figure 7. Variation of normalized resistance as a function of combined stretching and twisting for rod-coated pristine PEDOT:PSS and its nanocomposite films on a chemically treated low-cost substrate. The inset shows the cracking of the composite film when combined stretching and twisting loads are applied. The arrows indicate the onset of material failure. Error bars with filled areas show the standard deviation for the set of experiments.

rates is an aggressive test. When combined with twisting, a complex state of mechanical strain develops which reduces interfacial traction between the film and substrate. Hence, the prepared laminates were found to fail at much lower strains and twist angles (in a combined test) compared to the laminates tested for stretching and twisting individually. From these results, it can be concluded that the electromechanical performance (in combined stretching and twisting) of thin film laminates on smooth RTV substrates solely depends on the deformation rates. Static conditions or lower deformation rates are required to achieve greater electromechanical performance in these tests.

3.4. Electromechanical behaviour under cyclic stretching and bending

The cyclic stretching behaviour of the prepared thin films is shown in Figure 8a. It can be seen that both types of films show nearly constant resistance when repeated stretching cycles up to 12% axial strain is applied. Pristine films are found to last six stretching cycles, which is slightly higher than composite films (four cycles). Also, the normalized resistance at the failure for both films remains close to one (0.987 for pristine and 1.006 for composite films), showing the stable resistive behaviour of both films.

The cyclic bending behaviour of prepared films is shown in Figure 8b. It can be seen that pristine films last longer (twenty-nine cycles) as compared to composite films (ten cycles). Also, the pristine films show nearly constant resistance up to twenty-one repeated bending cycles. After that, the films start cracking and delaminating, which leads to the unloading of the film as it leaves the substrate; hence, after twenty-two cycles, the normalized resistance becomes nearly unchanged. In the case of composite films, the normalized resistance increased after each bending cycle until it failed completely. In general, the different behaviour of composite films in each of these cyclic tests is because cyclic tests are fatigue-type tests. Therefore owing to their higher stiffness, the nanocomposite films showed slightly reduced performance than pristine films. Furthermore, results from previous research works indicated that the films produced on rough or patterned substrates exhibited higher electromechanical performance in cyclic tests such as bending. This is because the surface roughness features act like anchors which keep the functional film attached to the surface of the substrate in the cyclic tests [16–18, 51]. In addition to this, these roughness features also form micro trenches which contract on the application of applied strain [16] and keep the film intact and attached to the substrate. On the other hand, the laminates used in this study are produced by coating thin films on a chemically treated smooth substrate. The adhesion of the film in these laminates exists only due to the stickiness and chemical changes caused in the functional groups present within the substrate as described in our recent research work related to the RTV polymer [24]. Also, the cyclic tests reported in this study are dynamic (2 s^{-1} in cyclic stretching and 1.43 s^{-1} in cyclic bending) which resulted in higher strain rates during cyclic tests. These factors contribute to the lower performance of the prepared thin film laminates in cyclic tests.

3.5. Electromechanical behaviour under vibration

Figure 9 shows the vibration response of PEDOT:PSS and its composite films on three different cams of sizes 0.5, 1 and 3 mm, respectively. The size of the

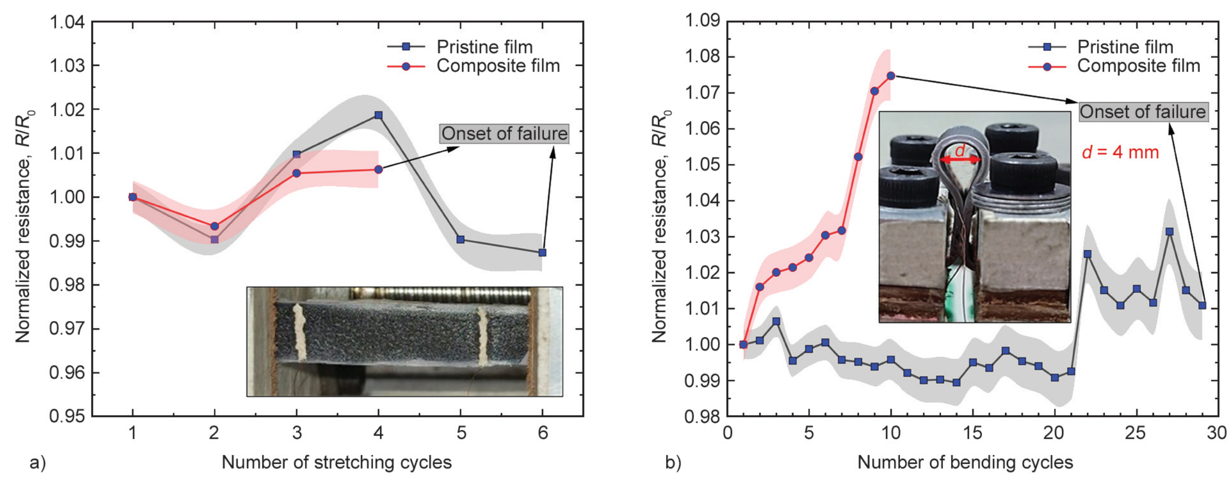

Figure 8. Variation of normalized resistance as a function of a) cyclic stretching, b) cyclic bending for rod-coated pristine PEDOT:PSS and its nanocomposite films on a chemically treated low-cost substrate. The inset shows the pristine PEDOT:PSS and its composite films under cyclic stretching and bending respectively. The arrows indicate the onset of material failure. Error bars with filled areas show the standard deviation for the set of experiments.

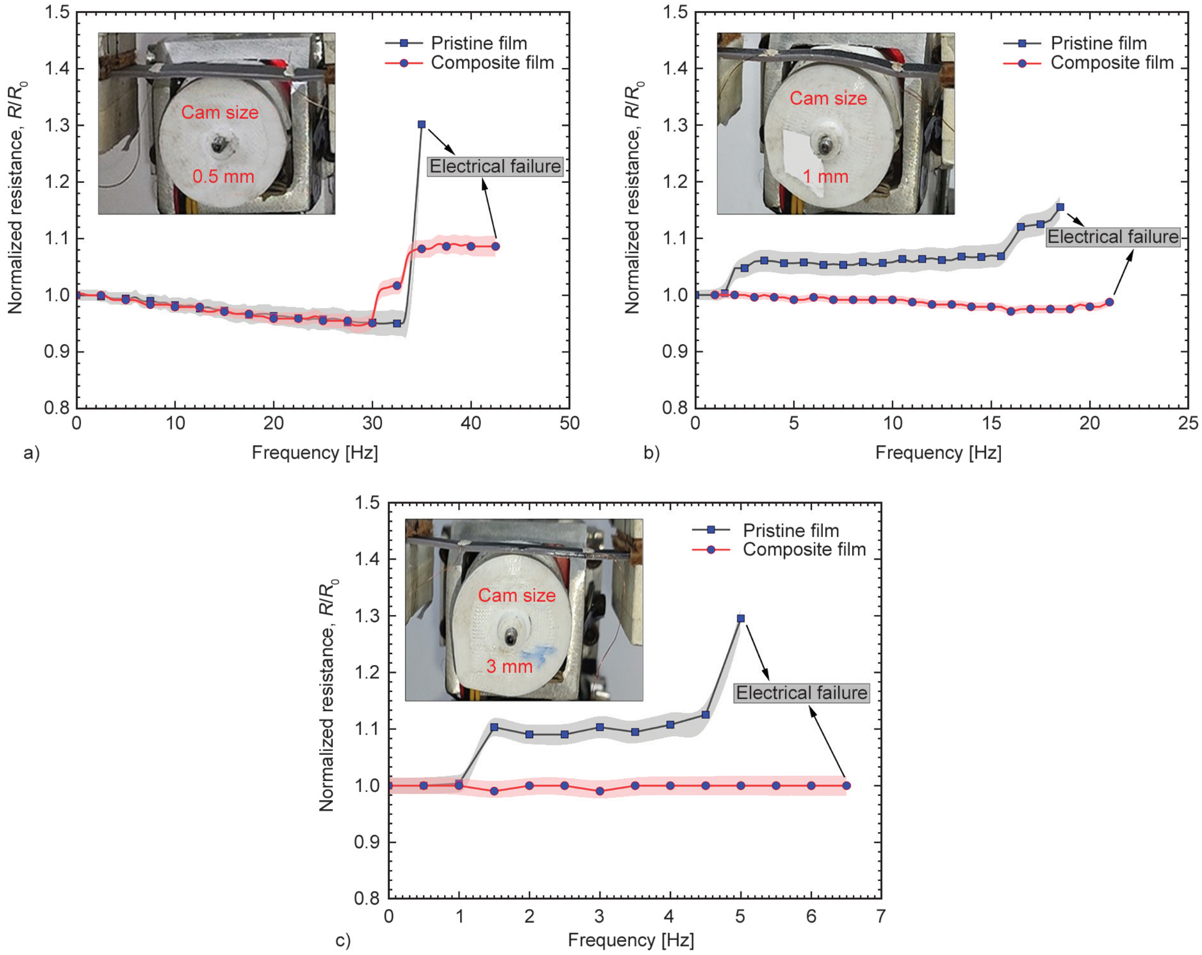

Figure 9. Variation of normalized resistance as a function of forced vibration for rod-coated pristine PEDOT:PSS and its nanocomposite films on a chemically treated low-cost substrate under the forced vibration amplitude of a) 0.5 mm, b) 1 mm, c) 3 mm. The inset shows the PEDOT:PSS based samples. The arrows indicate the complete electrical failure. Error bars with filled areas show the standard deviation for the set of experiments.

cam represents the maximum amplitude produced by it during forced vibrations. As it is evident from the vibration graphs for cam sizes 1 and 3 mm, the pristine films undergo a gradual change in resistance up to the failure whereas, the composite films maintain constant resistance. Also, the composite films withstand higher vibration frequencies than the pristine films for all three cam sizes. This shows that adding silver nanoplatelets improves the performance of composite films against forced vibrations, making them more stable than pristine films. In addition to this, the pristine films maintains their resistance at lower amplitudes (cam size 0.5 mm) up to an excitation frequency of 30 Hz. Furthermore, at higher amplitudes, both films fail at consistently lower frequencies, which shows that increasing the excitation amplitude impacts the electromechanical performance of substrate-bonded thin films.

3.6. Thermal stability and actuation behaviour

Figure 10 shows the variation of normalized resistance of the prepared thin films as a function of temperature. It can be seen that initially, up to 138 °C, the resistance of pristine PEDOT:PSS films remains nearly unchanged. After 138 °C, resistance increases until it reaches 2.18 times the initial resistance. On further increasing the temperatures, the resistance starts decreasing. This decrement is attributed towards the tunnelling effect in PEDOT:PSS, as reported by other authors [51–53].

Furthermore, the decrease in resistance continues until it reaches a constant resistance value of 1.60 times the initial one. After this point, a temperature change produces no change in resistance. This behaviour is caused by morphological changes produced at higher temperatures. At such high temperatures, the films

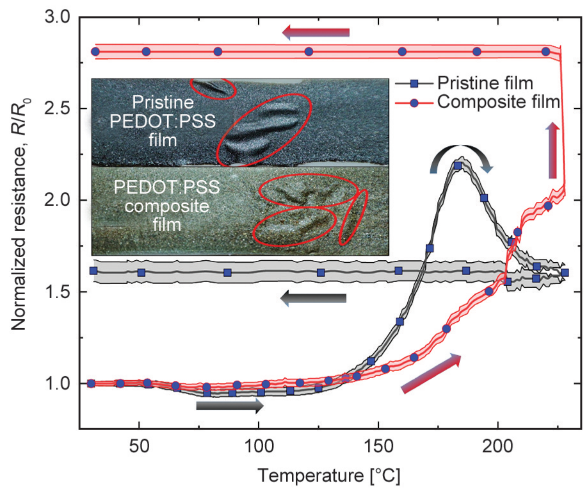

Figure 10. Variation of normalized resistance as a function of temperature for rod-coated pristine PEDOT:PSS and its nanocomposite films on a chemically treated low-cost substrate. The inset shows the morphological changes produced in the films at higher temperatures and caused a permanent change in the resistance of both films. Error bars with filled areas show the standard deviation for the set of experiments.

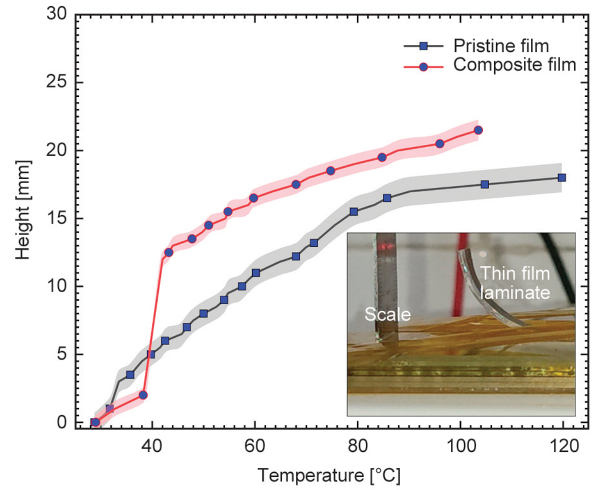

Figure 11. Thermal actuation behaviour of rod coated pristine PEDOT:PSS and its nanocomposite films on a chemically treated low-cost substrate. The inset shows the photographic image of the PEDOT:PSS nanocomposite-based thermal actuator. Error bars with filled areas show the standard deviation for the set of experiments.

were found to delaminate at different points, which caused a permanent change in resistance, as shown in the inset of the thermal behaviour graph. Also, the *N*,*N*-DMF present in the thin film material boiled at higher temperatures and thus contributed towards the permanent change in resistance of the laminate. Therefore, the resistance remains the same even after decreasing the temperatures down to room temperature. In composite films, the same type of behaviour was observed except for two observations. First, the composite films maintain constant resistance at slightly higher temperatures than pristine films (upto 153 °C). Second, due to the presence of metal nanoplatelets, the film's resistance keeps rising with increasing temperatures and reaches a higher resistance value which is 2.81 times the initial resistance at 220 °C. After that, the resistance remains constant and does not affect by the changing temperatures. Like pristine films, composite films also develop morphological changes which resist further change in resistance, as shown in the inset of the thermal behaviour graph.

The thermal actuation response of the prepared thin film laminates is shown in Figure 11. It can be seen that both types of laminates exhibit good actuation in response to the applied thermal gradient. The pristine laminates show linear actuation response up to 85 °C after which the laminates respond slowly to the applied temperature. The maximum actuation height of 18 mm was recorded at a temperature of 119.75 °C. In the case of composite laminates, a quick actuation response was observed initially. The laminate rapidly jumps from 2 mm (38.25 °C) to 12 mm (42 °C) after which a linear actuation response was observed. The maximum actuation height of 21.5 mm was recorded at a temperature of 103.5 °C. The fast actuation response of the composite laminates is attributed towards the addition of metal nanoplatelets which changes the thermal properties of the composite films coated on the RTV substrates. Therefore, from these results, it can be concluded that the as-prepared thin films can be used as a thermal actuator, switch or thermal valve in various MEMS-based devices and microfluidics applications.

4. Conclusions

This article presents the fabrication and electromechanical characterizations of PEDOT:PSS and its nanocomposite films on a chemically treated, cost-effective single-component polymer substrate. The films were fabricated by a low-cost non-vacuum-based rod coating method. The electromechanical performances of the films were checked by different mechanical and thermal tests. The results show that overall the laminates exhibit good mechanical performance on the RTV substrate. In stretching, the pristine and composite films remained functional up to

15 and 17% strain, respectively. In combined stretching and twisting, the pristine films survived to 1.94% strain at an angle of 84.4°, while the composite films lasted up to 4.86% strain at 218.3°. In twisting, the pristine films lasted up to 349° in slow and 189° in fast twisting while the composite films were twisted up to 360 and 351° in the slow and fast twisting tests, respectively. The laminates showed reduced electromechanical performance in cyclic tests, which is primarily caused by the absence of roughness features on the substrate. In vibration testing, it was found that the higher cam sizes reduce the performance of the films against forced vibrations. The minimum and maximum frequencies for pristine and composite films were found to be 5 and 42 Hz respectively. The prepared laminates also show good thermal stability up to 187 °C (pristine films) and 227 °C (composite films) without any thermal degradation. In summary, the as-fabricated thin film laminates are shown to have versatile applications such as stretchable, bendable, and twistable sensors, thermal sensors, actuators, switches and valves, and vibration-tolerant devices. These applications can be useful for future low-cost stretchable and flexible MEMS-based applications.

Acknowledgements

The authors would like to extend their gratitude to the NED University of Engineering and Technology for supporting this research work.

References

[1] Eun K., Chon M-W., Yoo T-H., Song Y-W., Choa S-H.: Electromechanical properties of printed copper ink film using a white flash light annealing process for flexible electronics. Microelectronics Reliability, **55**, 838–845 (2015).
https://doi.org/10.1016/j.microrel.2014.12.015

[2] Glushko O., Cordill M. J., Klug A., List-Kratochvil E. J. W.: The effect of bending loading conditions on the reliability of inkjet printed and evaporated silver metallization on polymer substrates. Microelectronics Reliability, **56**, 109–113 (2016).
https://doi.org/10.1016/j.microrel.2015.10.007

[3] Ma L., Lu W.: Carbon nanotube film based flexible bidirectional strain sensor for large deformation. Materials Letters, **260**, 126959 (2020).
https://doi.org/10.1016/j.matlet.2019.126959

[4] Nauman M. M., Mehdi M., Hussain D., Zaini J. H., Abu Bakar M. S., Askari H., Baig B. A., Rehman A., Abbas H., Hussain Z., Zaki D.: Stretchable and flexible thin films based on expanded graphite particles. Processes, **8**, 961 (2020).
https://doi.org/10.3390/pr8080961

[5] Gao Z., Ren B., Fang Z., Kang H., Han J., Li J.: Accurate recognition of object contour based on flexible piezoelectric and piezoresistive dual mode strain sensors. Sensors and Actuators A: Physical, **332**, 113121 (2021).
https://doi.org/10.1016/j.sna.2021.113121

[6] Mavlonov A., Chantana J., Nishimura T., Kawano Y., Inoue M., Hamada N., Masuda T., Minemoto T.: Superstrate-type flexible and bifacial Cu(In,Ga)Se_2 thin-film solar cells with In_2O_3:SnO_2 back contact. Solar Energy, **211**, 725–731 (2020).
https://doi.org/10.1016/j.solener.2020.10.019

[7] Mukherjee S., Albertengo A., Djenizian T.: Beyond flexible-Li-ion battery systems for soft electronics. Energy Storage Materials, **42**, 773–785 (2021).
https://doi.org/10.1016/j.ensm.2021.08.020

[8] Han X., Jiang D., Qu X., Bai Y., Cao Y., Luo R., Li Z.: A stretchable, self-healable triboelectric nanogenerator as electronic skin for energy harvesting and tactile sensing. Materials, **14**, 1689 (2021).
https://doi.org/10.3390/ma14071689

[9] Yin J., Kim J., Lee H. U., Park J. Y.: Highly conductive and flexible thin film electrodes based on silver nanowires wrapped carbon fiber networks for supercapacitor applications. Thin Solid Films, **660**, 564–571 (2018).
https://doi.org/10.1016/j.tsf.2018.05.043

[10] Sriwichai S., Phanichphant S.: Fabrication and characterization of electrospun poly(3-aminobenzylamine)/functionalized multi-walled carbon nanotubes composite film for electrochemical glucose biosensor. Express Polymer Letters, **16**, 439–450 (2022).
https://doi.org/10.3144/expresspolymlett.2022.32

[11] Valadbeigi E., Modarresi-Alam A. R., Noroozifar M., Rezvani A. R.: Synthesis and characterization of new nanocomposites of [poly(o-toluidine)]/(WO_3 nanoparticles) and their application in novel hybrid solar cells. Express Polymer Letters, **16**, 939–959 (2022).
https://doi.org/10.3144/expresspolymlett.2022.69

[12] Motora K. G., Wu C-M., Rani G. M., Yen W-T.: Effect of ZnO particle size on piezoelectric nanogenerators and mechanical energy harvesting. Express Polymer Letters, **16**, 1208–1227 (2022).
https://doi.org/10.3144/expresspolymlett.2022.88

[13] Borghetti M., Serpelloni M., Sardini E., Pandini S.: Mechanical behavior of strain sensors based on PEDOT:PSS and silver nanoparticles inks deposited on polymer substrate by inkjet printing. Sensors and Actuators A: Physical, **243**, 71–80 (2016).
https://doi.org/10.1016/j.sna.2016.03.021

[14] Jang H-H., Park J-S., Choi B.: Flexible piezoresistive pulse sensor using biomimetic PDMS mold replicated negatively from shark skin and PEDOT:PSS thin film. Sensors and Actuators A: Physical, **286**, 107–114 (2019). https://doi.org/10.1016/j.sna.2018.12.015

[15] Cui Y. J., Wang B. L., Wang K. F.: Energy conversion performance optimization and strength evaluation of a wearable thermoelectric generator made of a thermoelectric layer on a flexible substrate. Energy, **229**, 120694 (2021). https://doi.org/10.1016/j.energy.2021.120694

[16] Mehdi S. M., Jo J., Doh Y. H., Dang H. W., Choi K. H.: Stretchable and flexible resistive behavior of poly(3,4-ethylenedioxythiophene):poly(styrenesulfonate) thin film on ultra-low modulus polydimethylsiloxane with trench-type roughness. Journal of Polymer Science Part B: Polymer Physics, **53**, 226–233 (2014). https://doi.org/10.1002/polb.23615

[17] Mehdi S. M., Akhtar M., Qamar S. Z.: Electromechanical response of delaminating polymer thin films on rough elastomeric substrate. Journal of Elastomers and Plastics, **49**, 696–705 (2017). https://doi.org/10.1177/0095244316687352

[18] Mehdi M., Akhtar M., Hussain A., Nauman M., Alothmany D. S., Ahmed I., Choi K-H.: Dip coated stretchable and bendable PEDOTPSS films on low modulus micro-bumpy PDMS substrate. Journal of Polymer Engineering, **38**, 469–474 (2018). https://doi.org/10.1515/polyeng-2017-0081

[19] Tan Z., Li H., Huang Y., Gong X., Qi J., Li J., Chen X., Ji D., Lv W., Li L., Hu W.: Breathing-effect assisted transferring large-area PEDOT:PSS to PDMS substrate with robust adhesion for stable flexible pressure sensor. Composites Part A: Applied Science and Manufacturing, **143**, 106299 (2021). https://doi.org/10.1016/j.compositesa.2021.106299

[20] Zhao X., Wang W., Wang Z., Wang J., Huang T., Dong J., Zhang Q.: Flexible PEDOT:PSS/polyimide aerogels with linearly responsive and stable properties for piezoresistive sensor applications. Chemical Engineering Journal, **395**, 125115 (2020). https://doi.org/10.1016/j.cej.2020.125115

[21] Wang J-C., Karmakar R. S., Lin T-H., Wu M-C., Chang K-H.: Reaction-inhibited interfacial coating between PEDOT:PSS sensing membrane and ITO electrode for highly-reliable piezoresistive pressure sensing applications. Journal of Taiwan Institute of Chemical Engineers, **126**, 297–306 (2021). https://doi.org/10.1016/j.jtice.2021.07.004

[22] He J., Zhang Y., Zhou R., Meng L., Chen T., Mai W., Pan C.: Recent advances of wearable and flexible piezoresistivity pressure sensor devices and its future prospects. Journal of Materiomics, **6**, 86–101 (2020). https://doi.org/10.1016/j.jmat.2020.01.009

[23] Xie K., Wei B.: Materials and structures for stretchable energy storage and conversion devices. Advanced Materials, **26**, 3592–3617 (2014). https://doi.org/10.1002/adma.201305919

[24] Khan S. T., Akhtar M., Mehdi M., Malik N., Hashmi S., Butt F.: Characterizations of a cost-effective single component polymer for stretchable and flexible microelectromechanical systems applications. Journal of Testing and Evaluation, **51**, 495–507 (2022). https://doi.org/10.1520/JTE20220161

[25] Cheng T., Zhang Y., Lai W-Y., Huang W.: Stretchable thin-film electrodes for flexible electronics with high deformability and stretchability. Advanced Materials, **27**, 3349–3376 (2015). https://doi.org/10.1002/adma.201405864

[26] Mehdi S. M., Cho K. H., Kang C. N., Choi K. H.: Stretchability of silver films on thin acid-etched rough polydimethylsiloxane substrates fabricated by electrospray deposition. Journal of Electronic Materials, **44**, 2514–2521 (2015). https://doi.org/10.1007/s11664-015-3813-6

[27] Mehdi S. M., Akhtar M., Hussain A., Alothmany D. S., Choi K-H.: Electromechanical response of dip-coated silver films on micro-bumpy polymer surface. Arabian Journal for Science and Engineering, **42**, 1903–1908 (2017). https://doi.org/10.1007/s13369-016-2358-1

[28] Mehdi M., Chandio A., Akhtar M., Khan Z., Zaman A., Muhammad A.: Silver nano platelet films on soft micro grating surface. Microelectronics International, **36**, 1–7 (2019). https://doi.org/10.1108/MI-07-2018-0044

[29] Hoek I., Tho F., Arnold W. M.: Sodium hydroxide treatment of PDMS based microfluidic devices. Lab on a Chip, **10**, 2283–2285 (2010). https://doi.org/10.1039/C004769D

[30] Hemmilä S., Cauich-Rodríguez J. V., Kreutzer J., Kallio P.: Rapid, simple, and cost-effective treatments to achieve long-term hydrophilic PDMS surfaces. Applied Surface Science, **258**, 9864–9875 (2012). https://doi.org/10.1016/j.apsusc.2012.06.044

[31] Wu X., Li X., Hao L., Wen X., Lan L., Yuan X., Zhang Q.: Effect of vulcanization temperature and humidity on the properties of RTV silicone rubber. IOP Conference Series: Materials Science and Engineering, **207**, 012011 (2017). https://doi.org/10.1088/1757-899X/207/1/012011

[32] Pradela-Filho L. A., Araújo D. A. G., Takeuchi R. M., Santos A. L.: Nail polish and carbon powder: An attractive mixture to prepare paper-based electrodes. Electrochimica Acta, **258**, 786–792 (2017). https://doi.org/10.1016/j.electacta.2017.11.127

[33] Araújo D. A. G., Camargo J. R., Pradela-Filho L. A., Lima A. P., Muñoz R. A. A., Takeuchi R. M., Janegitz B. C., Santos A. L.: A lab-made screen-printed electrode as a platform to study the effect of the size and functionalization of carbon nanotubes on the voltammetric determination of caffeic acid. Microchemical Journal, **158**, 105297 (2020). https://doi.org/10.1016/j.microc.2020.105297

[34] Camargo J. R., Andreotti I. A. A., Kalinke C., Henrique J. M., Bonacin J. A., Janegitz B. C.: Waterproof paper as a new substrate to construct a disposable sensor for the electrochemical determination of paracetamol and melatonin. Talanta, **208**, 120458 (2020).
https://doi.org/10.1016/j.talanta.2019.120458

[35] Camargo J. R., Orzari L. O., Araújo D. A. G., de Oliveira P. R., Kalinke C., Rocha D. P., dos Santos A. L., Takeuchi R. M., Munoz R. A. A., Bonacin J. A., Janegitz B. C.: Development of conductive inks for electrochemical sensors and biosensors. Microchemical Journal, **164**, 105998 (2021).
https://doi.org/10.1016/j.microc.2021.105998

[36] Liu D., Hong G.: Wearable electromechanical sensors and its applications. in 'Wearable devices' (ed.: Nasiri N.) IntechOpen, London, **1**, 75–98 (2019).
https://doi.org/10.5772/intechopen.85098

[37] di Vito D., Mosallaei M., Khorramdel B., Kanerva M., Mäntysalo M.: Mechanically driven strategies to improve electromechanical behaviour of printed stretchable electronic systems. Scientific Reports, **10**, 12037 (2020).
https://doi.org/10.1038/s41598-020-68871-w

[38] Cordill M. J., Glushko O., Putz B.: Electro-mechanical testing of conductive materials used in flexible electronics. Froniers in Materials, **3**, 11 (2016).
https://doi.org/10.3389/fmats.2016.00011

[39] Mehdi S. M., Dang H. W., Kang C. N., Choi K. H.: Resistive behaviour of silver nanoparticle films on ultralow modulus polydimethylsiloxane with trench type roughness. Journal of Physics D: Applied Physics, **48**, 015303 (2015).
https://doi.org/10.1088/0022-3727/48/1/015303

[40] Yang H., Yao X., Zheng Z., Gong L., Yuan L., Yuan Y., Liu Y.: Highly sensitive and stretchable graphene-silicone rubber composites for strain sensing. Composites Science and Technology, **167**, 371–378 (2018).
https://doi.org/10.1016/j.compscitech.2018.08.022

[41] Luo R., Li X., Li H., Du B., Zhou S.: A stretchable and printable PEDOT:PSS/PDMS composite conductors and its application to wearable strain sensor. Progress in Organic Coatings, **162**, 106593 (2022).
https://doi.org/10.1016/j.porgcoat.2021.106593

[42] Li T., Huang Z., Suo Z., Lacour S. P., Wagner S.: Stretchability of thin metal films on elastomer substrates. Applied Physics Letters, **85**, 3435–3437 (2004).
https://doi.org/10.1063/1.1806275

[43] Xiao W., Deng H., Zou S., Ren Y., Tang D., Lei M., Xiao C., Zhou X., Chen Y.: Effect of roughness of substrate and sputtering power on the properties of TiN coatings deposited by magnetron sputtering for ATF. Journal of Nuclear Materials, **509**, 542–549 (2018).
https://doi.org/10.1016/j.jnucmat.2018.07.011

[44] Artieda A., Barbieri M., Sandu C. S., Muralt P.: Effect of substrate roughness on *c*-oriented AlN thin films. Journal of Applied Physics, **105**, 024504 (2009).
https://doi.org/10.1063/1.3068309

[45] Kamat S. V., Puri V., Puri R. K.: The effect of film thickness on the structural properties of vacuum evaporated poly(3-methylthiophene) thin films. ISRN Polymer Science, **2012**, 570363 (2012).
https://doi.org/10.5402/2012/570363

[46] Rao T. P., Santhoshkumar M. C.: Effect of thickness on structural, optical and electrical properties of nanostructured ZnO thin films by spray pyrolysis. Applied Surface Science, **255**, 4579–4584 (2009).
https://doi.org/10.1016/j.apsusc.2008.11.079

[47] Sim G-D., Won S., Lee S-B.: Tensile and fatigue behaviors of printed Ag thin films on flexible substrates. Applied Physics Letters, **101**, 191907 (2012).
https://doi.org/10.1063/1.4766447

[48] Hamasha M. M., Alzoubi K., Lu S.: Behavior of sputtered indium-tin-oxide thin film on poly-ethylene terephthalate substrate under stretching. IEEE/OSA Journal of Display Technology, **7**, 426–433 (2011).
https://doi.org/10.1109/JDT.2011.2131634

[49] Lacour S. P., Wagner S., Huang Z., Suo Z.: Stretchable gold conductors on elastomeric substrates. Applied Physics Letters, **82**, 2404–2406 (2009).
https://doi.org/10.1063/1.1565683

[50] Lambricht N., Pardoen T., Yunus S.: Giant stretchability of thin gold films on rough elastomeric substrates. Acta Materialia, **61**, 540–547 (2013).
https://doi.org/10.1016/j.actamat.2012.10.001

[51] Mehdi M., Cho K. H., Choi K. H.: Versatile poly(3,4-ethylenedioxythiophene) poly(styrenesulfonate) films on polydimethylsiloxane substrates having random micro ridges: Study of resistive behaviors of a polymer-polymer laminate. Journal of Applied Polymer Science, **132**, 41235 (2015).
https://doi.org/10.1002/app.41235

[52] Ali M. Z., Ishak K. M. K., Zawawi M. A. M., Jaafar M., Ahmed Z.: Tunneling percolation mechanism of conductivity for PEDOT:PSS in hydrophilic PDMS composite for the fabrication of highly sensitive strain sensors. Macromolecular Chemistry and Physics, **223**, 2200077 (2022).
https://doi.org/10.1002/macp.202200077

[53] Seo D-H., Im K., Song H.: High-temperature electronic transport properties of PEDOT:PSS top-contact molecular junctions with oligophenylene dithiols. Crystals, **12**, 962 (2022).
https://doi.org/10.3390/cryst12070962